

Finding Conditions to Process Hydrate Crystals and Amorphous Solids of Disodium Guanosine 5'-Monophosphate by an Antisolvent Crystallization Process

Jungsuk Kim* and Joachim Ulrich

A screening of amorphous, heptahydrate, and tetrahydrate forms of disodium guanosine 5'-monophosphate is investigated using an antisolvent crystallization process with the aim to selectively produce each solid form. The concentrations of the solution and solid forms are monitored by in situ Raman spectroscopy using a calibration tool. Particle sizes and particle counts are measured with elapsed time by a focal beam reflection measurement. Concentrations of amorphous and hydrates phases are determined using in-line measurement techniques. The variables studied are temperature, initial concentration, addition rate, and solvent fraction. The results demonstrate that transformation from amorphous to hydrate forms consists of four stages, which are the nucleation of the amorphous form, predissolution of amorphous form, the nucleation of hydrate crystal and dissolution of amorphous solid, and the growth of hydrate crystal. The rate-controlling step, in this case, is the dissolution of amorphous form. Transformation between heptahydrate to tetrahydrate crystals is a nucleation-growth-controlled step. It is possible to obtain selectively the solid forms of disodium guanosine 5'-monophosphate by referring to the supersaturation and solubility data.

dissolution.^[3–5] Hydrates can be described in terms of their stoichiometry relative to the host molecule; i.e., they are either stoichiometric or nonstoichiometric.^[6] In general, amorphous and hydrate forms of the same material exhibit different physical properties such as compressibility, melting point, and solubility, which can greatly affect the performance of the material thereafter.^[6,7] Therefore, it is important to control the manufacturing process to produce selectively the desired solid forms.

According to Ostwald's rule of stages,^[8] a solution-mediated crystallization process^[9] frequently transforms the crystalline forms and only allows changes from metastable forms to stable forms, making it difficult to prepare metastable forms. Therefore, it is important to grasp which operation factors influence the transformation. The


transformation is caused by the difference in solubility between the two forms or various mechanisms depending on the supersaturation conditions. The crystallization conditions for the production of the pure metastable form can also be set according to the supersaturation conditions.^[10] Therefore, the generation of the amorphous form can also be established by this method.^[11,12] When an amorphous form is suspended in a saturated solution, a transformation into a stable crystalline form can occur. Knowing the supersaturation limit is essential for the selective crystallization of disodium guanosine 5'-monophosphate (GMP) solid forms that exist as tetrahydrates, heptahydrates, and amorphous forms.

GMP is an important material for RNA production, and is also used as an intermediate of pharmaceuticals and as a food additive.^[13,14] GMP is synthesized by fermentation and then purified by crystallizing the fermentation broth. Crystallization serves to control product qualities, such as the hydrate form and the purity. GMP exists in several hydrate forms and one amorphous form.^[4,5] The chemical structures of tetrahydrate and heptahydrate GMPs are shown in Figure S11 (Supporting Information). In order to understand transformation of the hydrate forms in solution-mediated crystallization, it is necessary to grasp the effect of supersaturation according to the crystallization conditions. In addition, previous studies on GMP crystallization have mainly

1. Introduction

In the process of preparing compounds that exist in various solid forms, either crystalline or amorphous forms, the selective production of a solid form is of interest.^[1,2] Thermodynamically, amorphous solids provide higher solubility and higher dissolution rate compared to crystalline forms. However, amorphous forms are often not wanted as they are not stable; they can be transformed during drying, processing, storage, or

J. Kim, J. Ulrich
ehe. Zentrum für Ingenieurwissenschaften
Nat Fak I
Martin-Luther-Universität Halle-Wittenberg
D-06099 Halle, Germany
E-mail: jungsuk.kim@natfak1.uni-halle.de

 The ORCID identification number(s) for the author(s) of this article can be found under <https://doi.org/10.1002/crat.202100176>

© 2022 The Authors. Crystal Research and Technology published by Wiley-VCH GmbH. This is an open access article under the terms of the Creative Commons Attribution-NonCommercial-NoDerivs License, which permits use and distribution in any medium, provided the original work is properly cited, the use is non-commercial and no modifications or adaptations are made.

DOI: 10.1002/crat.202100176

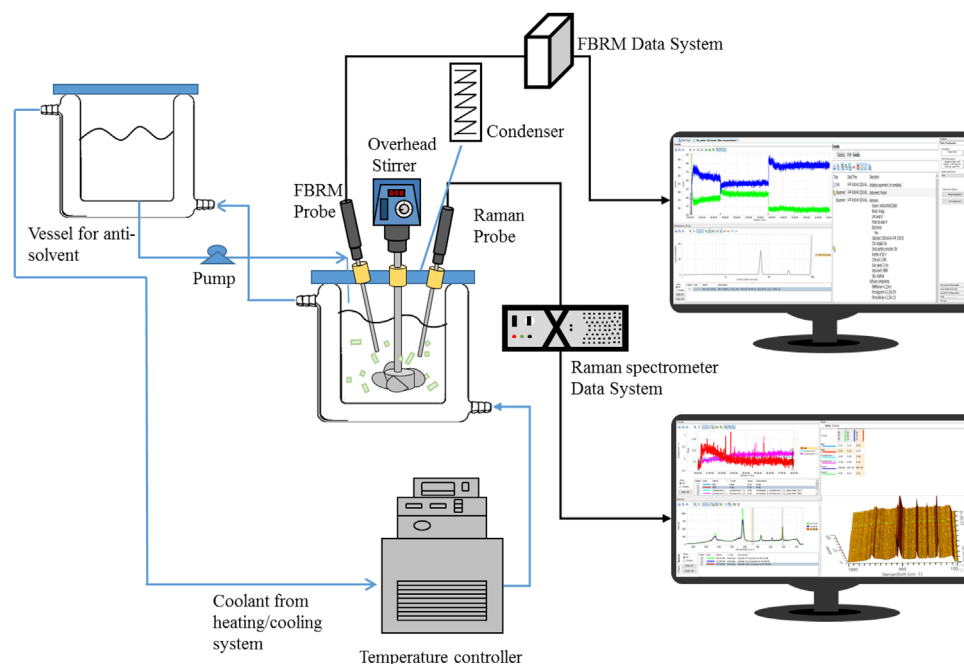


Figure 1. Experimental setup.

focused on the transformation of heptahydrate and amorphous forms.^[15–17] Several papers have reported crystallization of GMP with variables, such as solvent, temperature, and pH.^[15–19] However, studies on the relationship between supersaturation and the solid form measured in situ, and the crystallization of tetrahydrate GMP are lacking. In GMP manufacturing, the analysis of the mechanisms of transformation between hydrate and amorphous states and between hydrate and hydrate states is required. In addition, conditions must be established for the growth of the amorphous and the hydrates without transformation. Therefore, the purpose of this study is to measure in situ the supersaturation concentration, solid concentration, particle size, particle size distribution, and particle numbers with time, and to determine supersaturation limits for selective formation of amorphous, heptahydrate, and tetrahydrate solids. For this purpose, an in-line measurement was introduced, because it is difficult to measure the form and the concentration of the transformable phase by off-line analysis.

Solvent-mediated transformation studies can use a single measurement instrument, such as attenuated total reflectance Fourier transformed infra-red (ATR-FTIR),^[20] near infra-red (NIR),^[21] Raman,^[22] or focused beam reflectance measurement (FBRM),^[23,24] but in many cases use a combination of instruments to understand simultaneously complex mechanisms. In order to understand the hydrate formation and the transformation during operation, it is necessary to measure not only the solid form and concentration of the suspended solid state in solution, but also the change in solute concentration. Supersaturation is a nonequilibrium parameter affecting nucleation and crystal growth kinetics.^[25–27] Supersaturation is calculated from the difference between solubility and actual solution concentration, which is measured in real time by in-line Raman spectroscopy. Particle number, particle size distribution, and particle

size are measured by FBRM as they provide information on nucleation and growth during transformation. This study provides a method for selective manufacturing of solid form by studying the formation and transformation of amorphous, heptahydrate, and tetrahydrate of GMP by combining FBRM and Raman information analyzed on-line over time. The supersaturation limit of antisolvent crystallization was established according to the methanol/water ratio, initial concentration, antisolvent feed rate, and temperature. The controlling steps in the transformation of amorphous-to-hydrate solids and hydrate-to-hydrate crystals were studied.

2. Experimental Section

2.1. Setup

The experimental setup is shown in **Figure 1**. It consisted of a double jacket crystallizer, a mechanical stirrer, a Raman probe, an FBRM probe, a thermostatic controller, a vacuum filter, and drying equipment. Experiments were performed in a normal mode of antisolvent crystallization, which is the method to add antisolvent to solution. The crystallizer was a 400 mL cylindrical glass vessel equipped with a 4.5 cm marine-type propeller. The stirring speed was 400 rpm. The Raman probe and FBRM probe were mounted inside the crystallizer. The solution was prepared by dissolving GMP in water at 10 K higher than the operating temperature and then maintaining it at the same temperature for 1 h. Then, as an antisolvent, methanol was fed at a constant rate into the stirred solution using a syringe pump. A thermostat (Jeio Tech, HTRC-30) equipped with a programmable controller was used to keep the temperature constant. After the experiment, the solids were separated by filtration and dried in an oven at 45 °C for 10 h. The addition rate of the antisolvent was 0.9–38.0 g

min⁻¹. The methanol fraction in the mixed solvent was in the range of 0.3–0.8, and the temperature was set to 20–50 °C. The initial concentration was set to 0.1–0.3 g g⁻¹.

The measuring instrument consists of an FBRM spectrometer (model M400LF, Mettler Toledo, USA) and a Raman spectrometer (Kaiser Optical Systems, USA), which are in-line measuring instruments. In situ Raman measurements were used to measure changes in solute concentration, solid concentration, and solid form over time. FBRM was used to monitor particle formation and to observe changes in particle size and particle number in real time during the crystallization process.

2.2. Raman Spectroscopy and FBRM

Raman spectra were recorded using RXN Systems (Kaiser Optical Systems, Ann Arbor MI, USA) equipped with a light-emitting diode laser (785 nm, 450 mW). The spectral range was 100–1890 cm⁻¹ acquired with a spectral width of 4 cm⁻¹ and 5 s exposure. The concentrations of the solids and solutions were calibrated using iCRaman software (Mettler-Toledo, Switzerland). Analysis of the Raman spectra was performed by the absence and occurrence of the original peaks found in the spectrum of a single component. A multivariate partial least squares (PLS) model was used to calibrate for the concentrations of solids and solutions. Previous studies have already verified the solid form by Raman spectra and powder X-ray diffraction (PXRD) patterns.^[29] The RXN2 system made the instrument setup, data acquisition, and simple analysis.

An FBRM probe was used to monitor the nucleation, dissolution, and growth of the material. FBRM measured the chord length distribution (CLD) as the chord length was converted to particle size. Count data can be split into specific population regions in the size. FBRM data were recorded every 10 s, and count numbers were used as indications that nucleation occurred. The transformation process was monitored by the change in particle size and number. The number and size of particles of amorphous and hydrated forms were determined by FBRM. iControl FBRM software (Mettler-Toledo) was applied for data collection and analysis. In all experiments, the FBRM scan speed was 2 m s⁻¹. Chord lengths are defined as the length of the segments of a line embedded in specific phases of a material.^[30] Chord length distributions obtained with FBRM can be used similar to particle size distributions of laser diffraction and image analysis in different particle size ranges.^[31]

2.3. Characterization of Solids and Raman Calibration

Raman spectrum and calibration results for amorphous, heptahydrate, tetrahydrate forms, and the solution concentrations were already reported.^[29] PXRD patterns, Raman spectrum, and differential scanning calorimeter-thermo gravimetric analyzer (DSC-TGA) results of amorphous, tetrahydrate and heptahydrate forms are shown in Figures S12–S14 (Supporting Information), respectively.

The Raman spectra of the tetrahydrate are 367, 431, 502, 593, 680, 882, 984, 1326, 1495, 1632, and 1705 cm⁻¹. Of those, 882 cm⁻¹ was chosen as the characteristic peak of the tetrahydrate

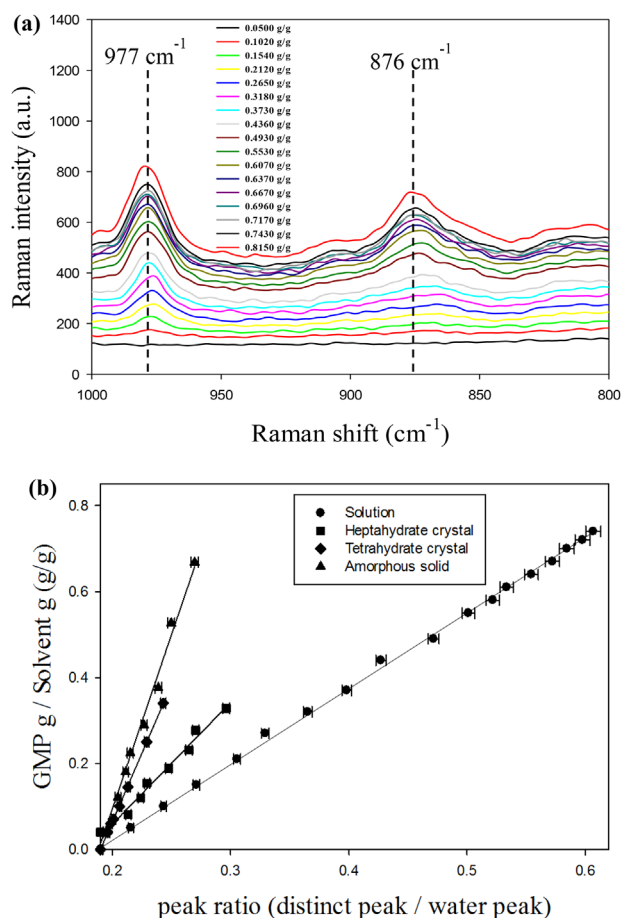


Figure 2. a) Raman intensities of solution concentration at 876 and 977 cm⁻¹ peaks. b) The results of the calibration for the concentrations of solution, amorphous solids, tetrahydrate crystals, and heptahydrate crystals. (R_{sgr} of linear regression analyses is 0.997.)

crystal. The Raman spectra of heptahydrate are 355, 387, 470, 592, 652, 832, 867, 974, 1009, 1057, 1090, 1185, 1418, 1495, and 1670 cm⁻¹. From them, 893 and 976 cm⁻¹ were selected as the characteristic peaks of heptahydrate. The Raman spectra of the amorphous form are 1741, 1587, 1480, 1372, 1328, 1025, 983, 880, 582, 503, 380, and 327 cm⁻¹. The characteristic peaks selected were 380 and 1480 cm⁻¹. Raman spectra of GMP dissolved in a solvent show distinct peaks at 876, 977, 1077, 1487, and 1581 cm⁻¹, while those of water are characterized at 373, 418, and 1742 cm⁻¹. Therefore, multiple intrinsic peaks of 876 and 977 cm⁻¹ were selected for the peaks of the GMP solution to obtain the calibration curve.

The calibration of the solution concentration at the 977 cm⁻¹ peak is shown in Figure 2a, while the Raman intensities of the solution concentrations for the peaks at 876 and 977 cm⁻¹ were shown. The Raman spectrum of the solution was measured in a solution, in which 0–80 g of GMP was completely dissolved in 100 g of a solvent. Raman spectra were collected at a solution concentration range of 0–0.8 g g⁻¹. The solution concentration was calculated using the intensity of the Raman peaks of dissolved GMP per peak of the solvent. The distinct peak of the solvent was at 418 cm⁻¹. A multivariate PLS model was used to correct

concentrations of solids and solutions. The calibration curves for the concentrations of solution, amorphous solids, tetrahydrate crystals, and heptahydrate crystals showed that the predicted concentration and the actual concentration were in a good agreement (Figure 2b). For a solid suspended in a saturated solution, a calibration curve for the solid was prepared using the Raman spectra. However, during the measurement of concentrations, a variation in the Raman spectra was found. Thus, the solid concentration was determined using the Raman spectra of the slurry before the transformation occurred. The calibration curves showed a correlation coefficient of 0.997.

3. Results and Discussion

3.1. Solubility and Supersaturation

In solution-mediated crystallization, supersaturation is the main parameter affecting the solid form that crystallizes.^[11,26] Previous studies have presented the solubility of heptahydrate, tetrahydrate, and amorphous forms of GMP as a function of a water-methanol fraction.^[29] The amorphous solubility was highest in the whole range of the solvent fraction. Below 45 °C, the solubilities of tetrahydrate and heptahydrate were close together with heptahydrate as somewhat lower one, while at 45 °C or higher, tetrahydrate was the slightly lower one. At 20 °C and a methanol fraction of >0.2, the solubility is in the order of amorphous > heptahydrate > tetrahydrate. At a methanol fraction of 0.3, the solubility difference between amorphous and heptahydrate and between heptahydrate and tetrahydrate are 0.0105 and 0.0065 g g⁻¹, respectively, and the solubility difference decreases as the methanol fraction increases. The supersaturation difference between the amorphous and the hydrates is clear. Thus, selective preparation of solid forms can be carried out by adjusting the temperature and the methanol/water ratio, based on the solubility and the supersaturation.

Although the solubility differences between the three forms are not very large, the metastable zone widths differ significantly. The metastable zone width depends on the supersaturation as a kinetic property. The solubility, on the other hand, is a thermodynamic property. Figure 3a,b shows schematic changes in metastable zone width with respect to methanol fraction and time in antisolvent crystallization, respectively. It serves as a guide for the formation and transformation of metastable forms. Therefore, from the understanding of the difference between saturation and supersaturation, a method for preparing selectively either a stable form or a metastable form without transformation can be proposed.

Supersaturation depends, besides the temperature, on the feed rate, initial concentration, and fraction of antisolvent in antisolvent crystallization. Therefore, amorphous, heptahydrate, and tetrahydrate forms can be selectively controlled by adjusting these variables. Figure 3a shows the metastable supersaturations $C_{met,a}$, $C_{met,h}$, and $C_{met,t}$ arbitrarily in the plots of solute concentration against methanol fraction. From this figure, during antisolvent crystallization at the initial concentration C1, the operating line meets $C_{met,a}$ to form an amorphous form; the concentration decreases; and an amorphous form is produced without transformation. At the initial concentration of C2, amorphous is first formed in $C_{met,a}$, and after a certain induction period,

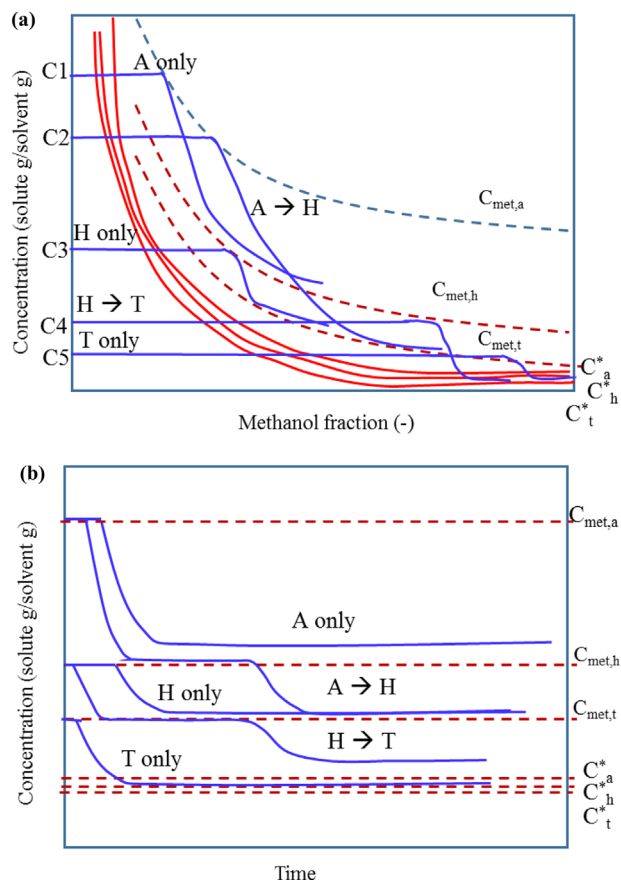


Figure 3. a) Schematic concentration changes with respect to methanol fraction. b) Schematic concentration changes with respect to time in antisolvent crystallization. (A, H, and T stand for amorphous, heptahydrate, and tetrahydrate, respectively.)

it meets $C_{met,h}$, in which amorphous is transformed into heptahydrate. At the initial concentration of C3, only the formation and growth of heptahydrate take place under the condition that it meets the limit line of the metastable zone of heptahydrate, $C_{met,h}$. At the initial concentration of C4, heptahydrate is first formed at $C_{met,h}$ and is transformed into tetrahydrate at $C_{met,t}$. At the initial concentration C5, only the formation and growth of tetrahydrate occur under the condition that it meets the limit line of the metastable zone of tetrahydrate, $C_{met,t}$. In addition, at the same concentration, a higher addition rate of the antisolvent leads to a greater supersaturation.

3.2. Selective Formation

There are various routes for formation of crystalline hydrates and the amorphous form. Antisolvent crystallization at an initial concentration of 0.1–0.3 g g⁻¹ and addition rates of 0.9–38 g min⁻¹ were carried out. Supersaturation was generated by adding antisolvent into the solution. In situ monitoring was observed by Raman spectroscopy. Raman spectra of eight cases are presented as 3D surface waterfalls in Figure 4.

Raman spectra with elapsed time are dramatically different in the range of 1890–200 cm⁻¹. As can be seen in Figure 4, the

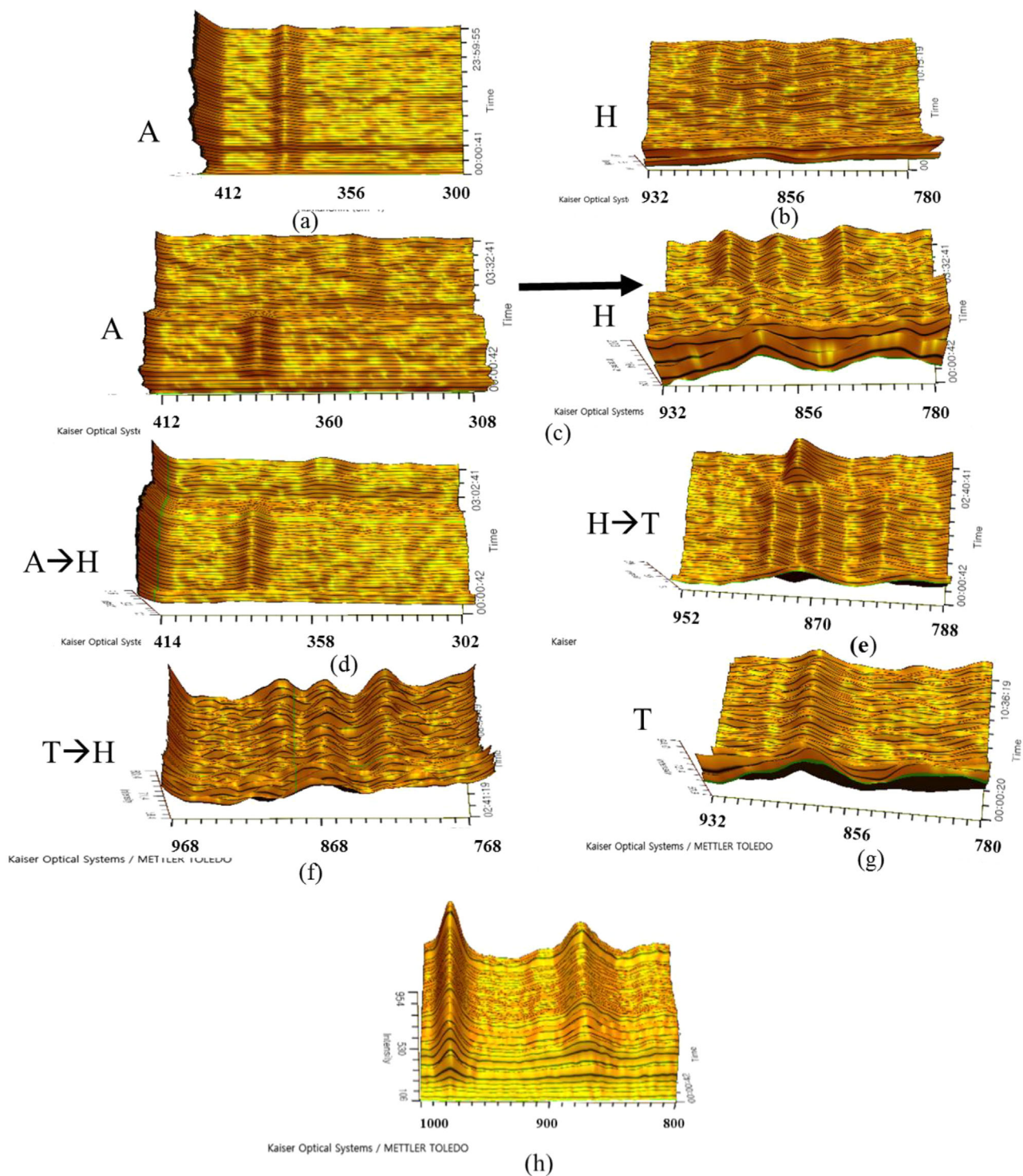


Figure 4. 3D surface waterfall Raman spectra in the regions of 300–412, 760–932, 302–414, and 800–1000 cm^{-1} , and during a) formation of the amorphous, b) formation of the heptahydrate, c,d) formation of the amorphous and transformation into the heptahydrate, e) formation of the heptahydrate and transformation into the tetrahydrate, f) formation of the tetrahydrate and transformation into the heptahydrate, g) crystallization of the tetrahydrate, and h) solution. (A, H, and T stand for amorphous, heptahydrate, and tetrahydrate, respectively.)

nucleation, the growth, and the transformation of amorphous, heptahydrate, and tetrahydrate were shown by Raman spectra in the range of 300–412, 760–932, and 302–414 cm^{-1} , respectively.

In Figure 4a, Raman spectra of solids, during operation, at a feed concentration of 0.3, a temperature of 20 °C, and an antisolvent fraction of 0.5 are presented as a 3D surface waterfall. The amorphous peak at 380 cm^{-1} was formed, and no transformation was observed for ≈ 24 h. Figure 4b shows heptahydrate peaks at 893 and 973 cm^{-1} , which were formed without transformation for 10 h. Figure 4c shows the amorphous peak at 380 cm^{-1} , which was formed first and transformed into heptahydrate with peaks at 893 and 973 cm^{-1} . Figure 4d shows the amorphous peak at 380 cm^{-1} , which was formed first and transformed into heptahydrate with a peak at 355 cm^{-1} . Raman spectra of heptahydrate peaks at 893 and 973 cm^{-1} were changed into that of the tetrahydrate peak at 882 cm^{-1} after 1.9 h (Figure 4e). Raman spectra of the tetrahydrate peak at 882 cm^{-1} were changed into that of the heptahydrate in the solid state at 1.5 h (see Figure 4f). At a feed concentration of 0.1, the tetrahydrate was directly nucleated without any transformation, which was evidenced by the appearance of the 882 cm^{-1} peak in Raman spectra. Raman spectra of this case are depicted in Figure 4g. Figure 4h shows Raman peaks of the solution concentrations at 867 and 977 cm^{-1} .

Therefore, it can be seen that the formation and transformation of the solid phase during the crystallization process can be quantified by Raman spectra. In this study, two in-line tools, Raman spectral analysis and FBRM, can clearly identify the solution-mediated transformation mechanism. Six case studies were conducted to prepare various forms of solids.

3.3. Case Studies for Transformations

3.3.1. Case for Amorphous to Heptahydrate State

Figure 5 shows Raman and FBRM data for the case of amorphous-to-heptahydrate transformation. It was carried out by antisolvent crystallization at 20 °C with a GMP/water ratio of 0.2, a methanol fraction of 0.33 in the solvent, and a methanol feed rate of 38 g min^{-1} . In this case, the results of Raman spectroscopy and FBRM can be divided into four sections: amorphous generation and growth, dissolution of amorphous solid, heptahydrate nucleation and transformation into heptahydrate, and heptahydrate growth.

Section I is the amorphous formation section. Solid formation is accomplished by adding methanol into the solution. The change of particle size is reflected in the FBRM's unweighted CLD, as shown in Figure 5b. The number of particles increased rapidly after generating supersaturation by methanol addition and then remained constant. The particle size also increased rapidly at the same time as the methanol added, and kept constant at about 11 μm . The width of the particle size distribution remained without change. It is clear that there were a large number of fine particles between 1 and 20 μm initially in the unweighted CLD. The amorphous concentration of 0.048 g g^{-1} , the solute concentration of 0.152 g g^{-1} in the solution (see Figure 5a), the number of counts, and the chord length were constant until 2800 s.

Section II is the pretransformation section. After 2900 s, the width of the particle size distribution did not change, and the peak began to decrease slightly. Accordingly, the number of particles decreased and the mean particle size was not changed (see Figure 5b). In addition, the number of fine particles between 1 and 20 μm underwent a relatively small change in the transformable form to prepare for the subsequent crystallization of the heptahydrate form (see Figure 5b,c). The concentrations of the solution and the amorphous solid were 0.152 and 0.048 g g^{-1} , respectively. Additionally, the pretransformation section is a step to prepare the supersaturation conditions to generate the heptahydrate nuclei.

Section III is the transformation section. The number of particles decreases rapidly, and the particle size increases due to the decrease in supersaturation and dissolution of the amorphous form with a higher solubility compared to the solubility of heptahydrate (see Figure 5b). For this reason, there is a moment at 5200 s in which the particle number increased slightly, and hence the particle size decreased slightly. At the same time, the concentration of the solution began to decrease. No dissolution of the amorphous solid was initially observed. After that, dissolution of amorphous solids and a sharp decrease in solution concentration occurred near 5900 s, and the solution supersaturation for heptahydrate steadily decreased, causing nucleation of heptahydrate. In the CLDs (see Figure 5c,d), a bimodal distribution curve was created as another peak appeared near 67 μm during the transformation process at 6900 and 7500 s. As a result, a bimodal distribution with peaks at 8.9 and 67 μm was shown. Therefore, the number of small particles (0–50 μm), which were amorphous solids, first increased, and then decreased due to the dissolution, which activated the crystal growth of heptahydrates.

In Section IV, due to the dissolution of the amorphous form and the growth of heptahydrate in the previous section, the particle number gradually decreased and the particle size increased to 67 μm . The increase in size was due to crystal growth of heptahydrate. In the particle size distribution, the amorphous particles disappeared completely, the bimodal distribution disappeared, and only crystals of heptahydrate around 67 μm existed (see Figure 5c,d). The solution concentration decreased from 0.2 to 0.069 g g^{-1} . In summary, this case consisted of amorphous formation, amorphous dissolution, amorphous to hydrate transformation, and hydrate crystal growth. Characteristically, an amorphous dissolution was discovered before transformation, and then the transformation process by nucleation of heptahydrate was revealed.

3.3.2. Case for Heptahydrate to Tetrahydrate

Figure 6 shows Raman and FBRM data for the case of heptahydrate-to-tetrahydrate transformation. It was carried out by antisolvent crystallization at 50 °C at a GMP/water ratio of 0.2, a methanol fraction of 0.5 in solvent, and a methanol feed rate of 38 g min^{-1} . In this case, the results of FBRM and Raman spectroscopy can be divided into three sections: nucleation and growth of heptahydrate, transformation from heptahydrate to tetrahydrate, and growth of tetrahydrate.

Section I represents the heptahydrate nucleation and growth. In crystallization, crystals of heptahydrate nucleate and grow

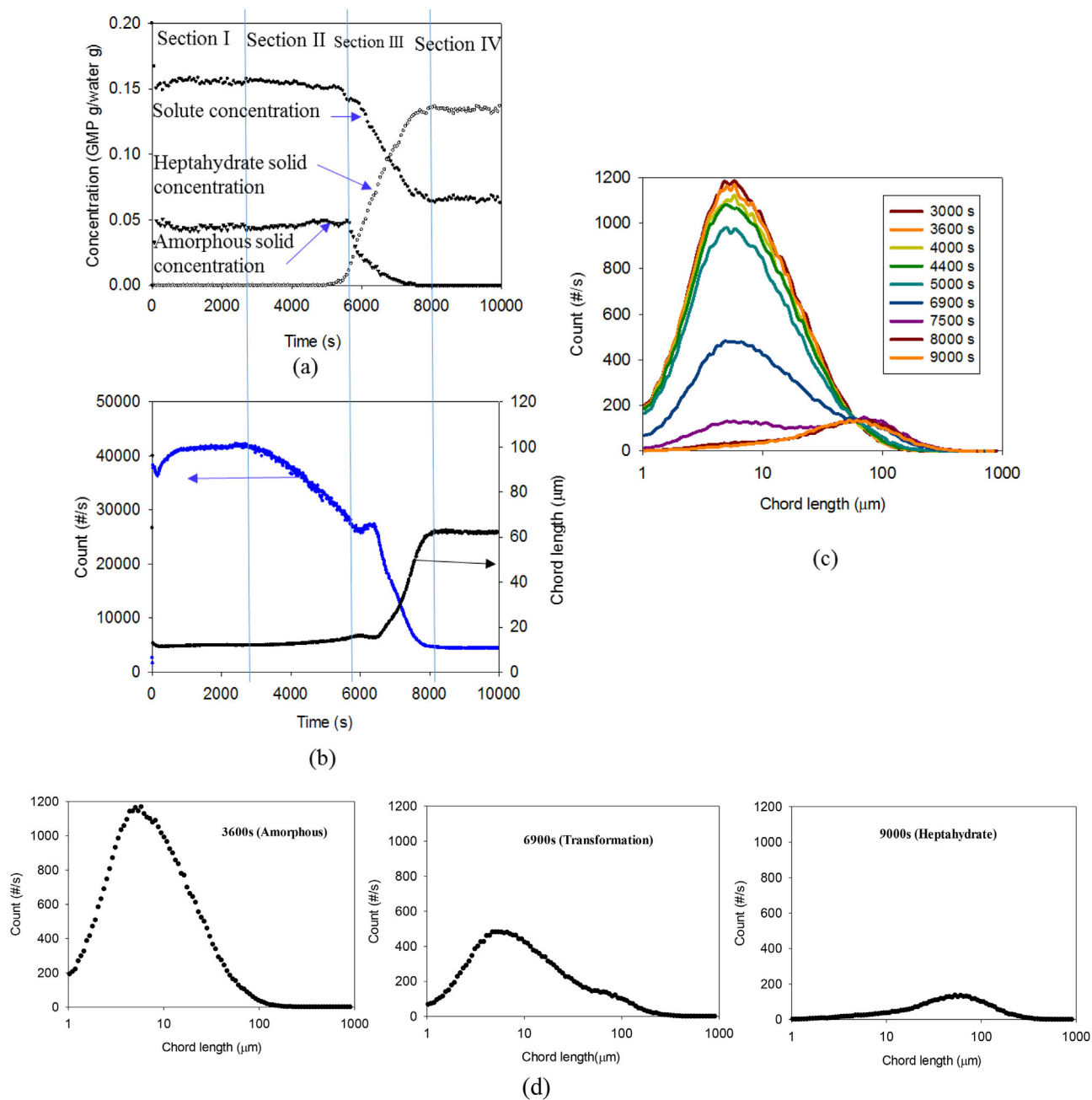


Figure 5. Raman and FBRM data for amorphous-to-heptahydrate transformation. a) Time–concentration profiles for solution, and amorphous, and heptahydrate solids. b) Counts and chord length from FBRM. c) Chord length distributions (CLDs) over time. d) CLDs during transformation.

by adding methanol into the solution. Upon the addition of methanol, supersaturation was achieved, and the number of particles increased rapidly and then remained at 8023 \# s^{-1} . The particle size also increased sharply at the same time as methanol addition and remained constant at about 43 \mu m . It was found that the width of the particle size distribution was not changed significantly in the range of $10\text{--}100 \text{ \mu m}$. The solution concentration decreased from 0.2 to 0.058 g g^{-1} when heptahydrate was formed, and the concentration of heptahydrate crystals increased to 0.142 g g^{-1} .

Section II represents nucleation of tetrahydrate and dissolution of heptahydrate (see Figure 6a,b). As shown in the solute concentration–time profile in Figure 6a, the solubilities of heptahydrate and tetrahydrate are similar, but the solubility of tetrahydrate is lower by 0.0052 g g^{-1} . After the induction period, the nucleation of tetrahydrate occurred rapidly as a result of the dissolution of heptahydrate due to the slightly higher solubility. For this reason, the particle number started to decrease suddenly at 5700 s and the particle size started to increase. According to the FBRM results, the crystal size increased from 43 to 48 \mu m during

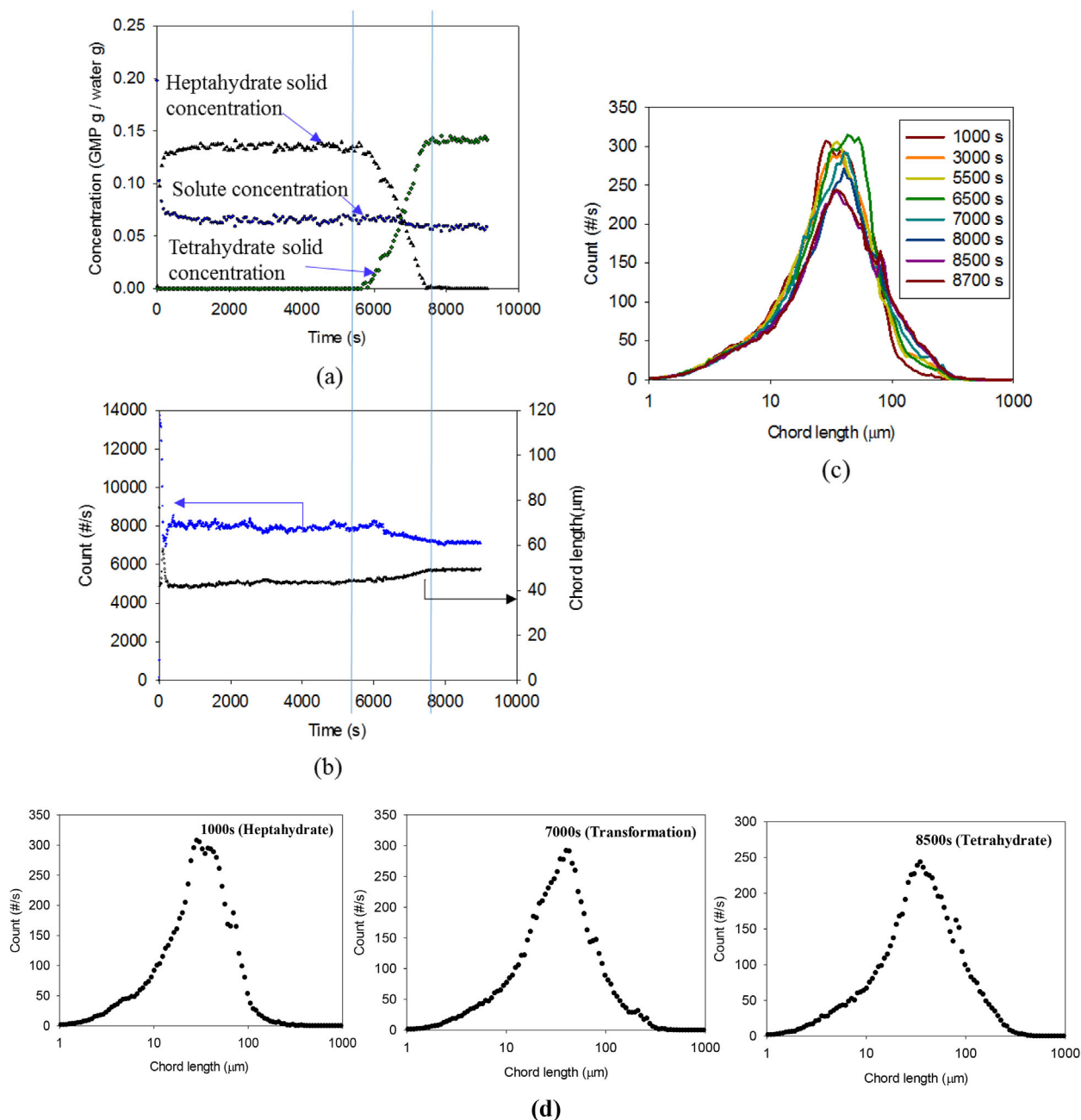


Figure 6. Raman and FBRM data for heptahydrate-to-tetrahydrate transformation. a) Time–concentration profiles for solution, and heptahydrate and tetrahydrate solids. b) Counts and chord length from FBRM. c) Chord length distributions (CLDs) over time. d) CLDs for transformation.

the transformation process (see Figure 6c,d). In the process, the number of particles decreased from 8023 # to 7600 # s⁻¹. Due to a small solubility difference, the solution concentration decreased by about 0.0071 g g⁻¹. No formation of an amorphous solid was observed.

Thereafter, the supersaturation for tetrahydrate formation steadily decreased, causing the growth of tetrahydrate in the state, where the dissolution of the heptahydrate near 6800 s does not result in a change in the solute concentration. Then the solute concentration decreased. In the particle size distribution, the peak near 43 μm was maintained without change during the transfor-

mation process. Therefore, the particle size distribution of heptahydrate was initially shown, but no change in the number of particles was observed by the nucleation of tetrahydrate in the fine particles (1–20 μm). Since there is a little difference in solubility between two hydrated crystals, the transformation process is driven by dissolution of heptahydrate crystals and growth of tetrahydrate crystals. Therefore, the number of transformed particles decreased, and the size increased by 5 μm (about 10%).

No clear change in particle size distribution was observed during the transformation process. Therefore, the nucleation of heptahydrate was not reflected in the distribution. In addition,

crystal growth caused the distribution to broaden to the right and the peak height to decrease slightly. From this phenomenon, transformation due to dissolution appears to be large and accompanied by crystal growth of tetrahydrate.

Section III is the tetrahydrate growth section. Due to the dissolution of the heptahydrate and the growth of the tetrahydrate, the particle number decreased slightly and the particle size increased up to 48 μm . The CLDs become gradually wider and indicate the growth of the tetrahydrate. In this case, nucleation of heptahydrate, transformation from heptahydrate to tetrahydrate, and growth of tetrahydrate were identified. Characteristically, there was a slight change in crystal size and little change in particle size distribution during the transformation process.

3.3.3. Case for Tetrahydrate to Heptahydrate

Figure 7 shows Raman and FBRM data for the case of tetrahydrate-to-heptahydrate transformation. It was carried out by antisolvent crystallization at 50 °C with a GMP/water ratio of 0.2, a methanol fraction of 0.333, and a methanol feed rate of 38 g min^{-1} . In this case, the results of FBRM and Raman spectroscopy can be divided into three sections: tetrahydrate nucleation and growth, heptahydrate nucleation and transformation, and heptahydrate growth.

Section I is the nucleation and growth of tetrahydrate section. The crystallization of tetrahydrate is achieved by adding methanol into the solution. After the addition of methanol to generate supersaturation, the number of particles increased rapidly and then was maintained at 2230 $\# \text{s}^{-1}$. The particle size also increased rapidly at the same time as methanol addition and was kept at about 41 μm . The width of the particle size distribution did not change significantly before 5100 s (see Figure 7c). The crystal distribution width of heptahydrate is narrower than that of tetrahydrate (see Figure 7d). The concentration of the solution decreased from 0.2 to 0.07 g g^{-1} , and the concentration of heptahydrate crystals was 0.13 g g^{-1} .

Section II is the section on nucleation of heptahydrate and dissolution of tetrahydrate (see Figure 7a,b). As can be seen in Figure 7a, crystallization of heptahydrate occurs rapidly due to the dissolution of tetrahydrate. It results from the slightly higher solution concentration compared to the solubility of the stable form (heptahydrate). For this reason, heptahydrate nucleation occurred instantaneously at 6000 s, and the particle number and particle size did not change. The concentration of the solution did not change either. No dissolution of the tetrahydrate solid was observed in the particle size distribution. After that, the crystal growth of tetrahydrate was induced in the state where no change in solution concentration was detected near 6000 s. The particle size distribution was maintained without changing the peak near 40 μm during the transformation process. Therefore, the particle size distribution of tetrahydrate appeared at first, but the number of particles increased in the fine particles (1–20 μm) due to nucleation of heptahydrate. Despite the dissolution of tetrahydrate and the growth of heptahydrate, the particle number and particle size did not change, and the number of coarse chord lengths (50–150 μm) was constant. In this process, nucleation of tetrahydrate, transformation from tetrahydrate to heptahydrate, and growth of heptahydrate were identified. Characteristically, the transforma-

tion process occurred with little change in particle size distribution, particle size, and number of particles.

According to the FBRM results, the particle size was almost constant at 40 μm during the transformation. There was little change in the number of particles. The reason is that the solubilities of heptahydrate and tetrahydrate are similar. The change in solution concentration had little effect with a decrease of about 0.001 g g^{-1} . There was no obvious change in the particle size distribution during the transformation. Therefore, the tetrahydrate crystals did not appear after transformation (see Figure 7c,d). It was observed that the particle size distribution was slightly widened to the right due to growth of heptahydrate crystals. From this phenomenon, it is expected that transformation by dissolution occurs on the solid surface and is accompanied by crystal growth.

3.4. Controlling Transformation Steps

3.4.1. Amorphous–Heptahydrate Transformation

As shown in Figure 5, the concentrations of solution, amorphous solid, and heptahydrate solid were presented. It was changed due to the formation of heptahydrate, a more stable form, and the solution concentration was reduced to 0.065 g g^{-1} . The concentration of the amorphous solid is 0.048 g g^{-1} . In the process of transformation, the supersaturation consumption rate by dissolution of the amorphous solid was 0.048 g g^{-1} per transformation time (2024 s), whereas the total formation–growth rate of heptahydrate was 0.135 g g^{-1} per transformation time (2024 s). The supersaturation consumption rate of the solution is 0.087 g g^{-1} per transformation time (2024 s). It is calculated as the difference between the solubility of the amorphous (0.152 g g^{-1}) and that of the heptahydrate (0.065 g g^{-1}). Therefore, this transformation process can be considered a dissolution-controlled transformation (frequently also called liquid-mediated phase change) because the nucleation-growth rate by supersaturation reduction is much higher than the amorphous dissolution rate. In the dissolution and growth mechanism, the overall dissolution and growth rate depends on the driving force, supersaturation. It is determined by the total surface area of the solid–liquid interface and the mass transfer rate constant from solution to crystal. In general, the growth rate is considered higher than the dissolution rate because there are both mass transfer resistances involved in the diffusion and surface integration steps.^[26,28] As shown in Figure 5b, the surface area of the amorphous solid–liquid interface is much higher than that of the heptahydrate during transformation. This is due to the fact that the amorphous form has a relatively large number of particles while relatively few crystals of heptahydrate are produced. This result supports the polymorphic transformation of methionine in batch crystallization.^[32,33]

3.4.2. Tetrahydrate–Heptahydrate Transformation

As shown in Figure 6, heptahydrate is formed after an induction period of 6000 s and tetrahydrate disappears at 8450 s. When heptahydrate was formed, the measured solubility was 0.067 g g^{-1} . Therefore, the supersaturation consumed by crystal growth of the

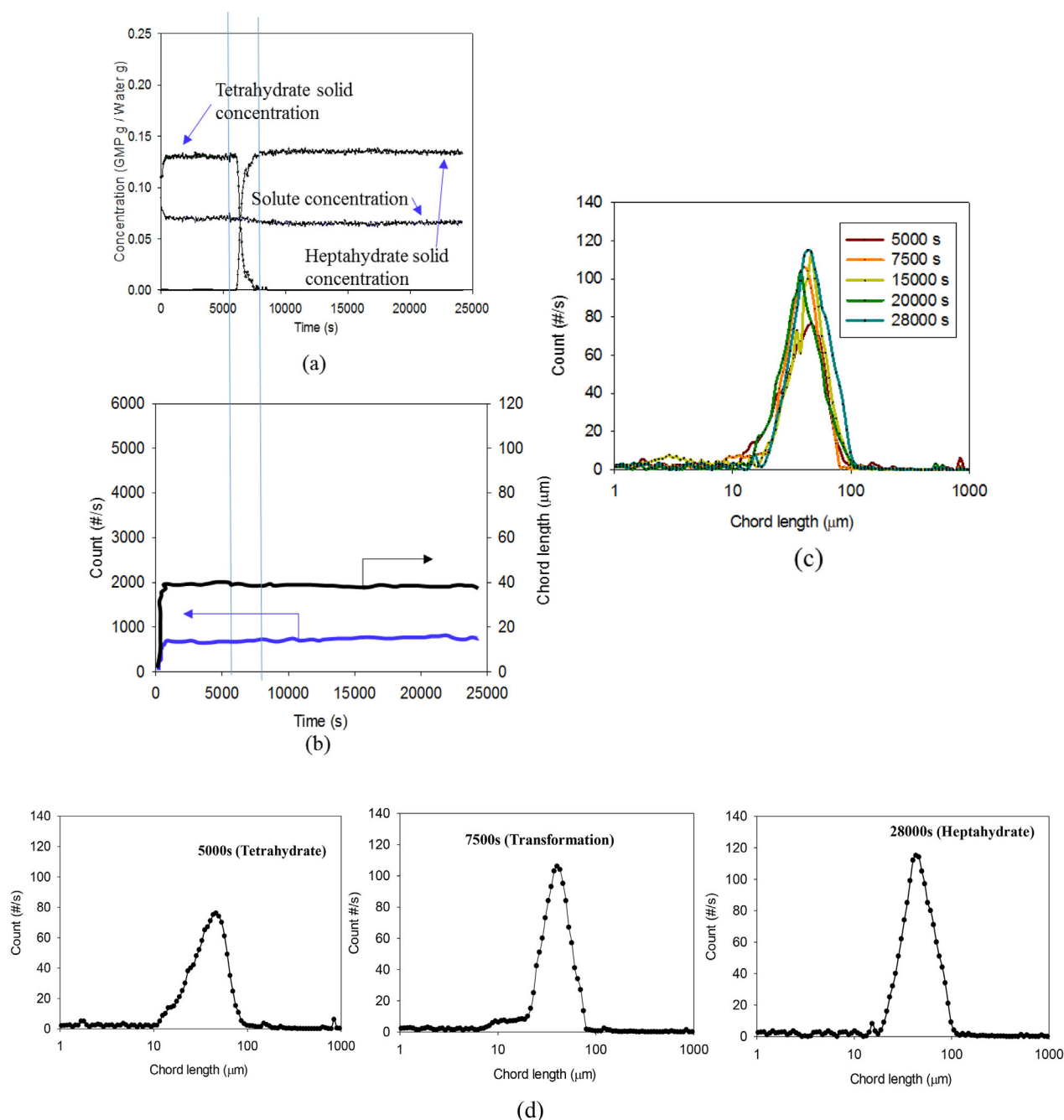


Figure 7. Raman and FBRM data for tetrahydrate-to-heptahydrate transformation. a) Time–concentration profiles for solution, and tetrahydrate and heptahydrate solids. b) Counts and chord length from FBRM over time. c) Chord length distributions (CLDs) over time. d) CLDs for transformation.

heptahydrate is about 0.132 g g^{-1} . The supersaturated consumption of the solution is 0.004 g g^{-1} . Therefore, the supersaturation rate in the solution was much lower than the consumption rate by dissolution of the tetrahydrate. There is also a plateau region of solution concentration of tetrahydrate. The solution concentration decreased when nucleation of heptahydrates started before solution concentration decreased and most of the tetrahydrates were dissolved. Therefore, this transformation can be considered a nucleation-growth-controlled transformation.

The solution concentration maintained the solubility of the tetrahydrate for 5850 s and remained constant until almost no solid form of the tetrahydrate remained in suspension. In the transformation, the supersaturation rate by crystal growth of heptahydrate was 0.137 g g^{-1} per 2735 s, and the total dissolution rate of the tetrahydrate was 0.132 g g^{-1} per 1527 s. Therefore, the rate of supersaturation consumption by nucleation growth is smaller than that by dissolution. This case demonstrates a nucleation-growth-controlling transformation step. The intrinsic

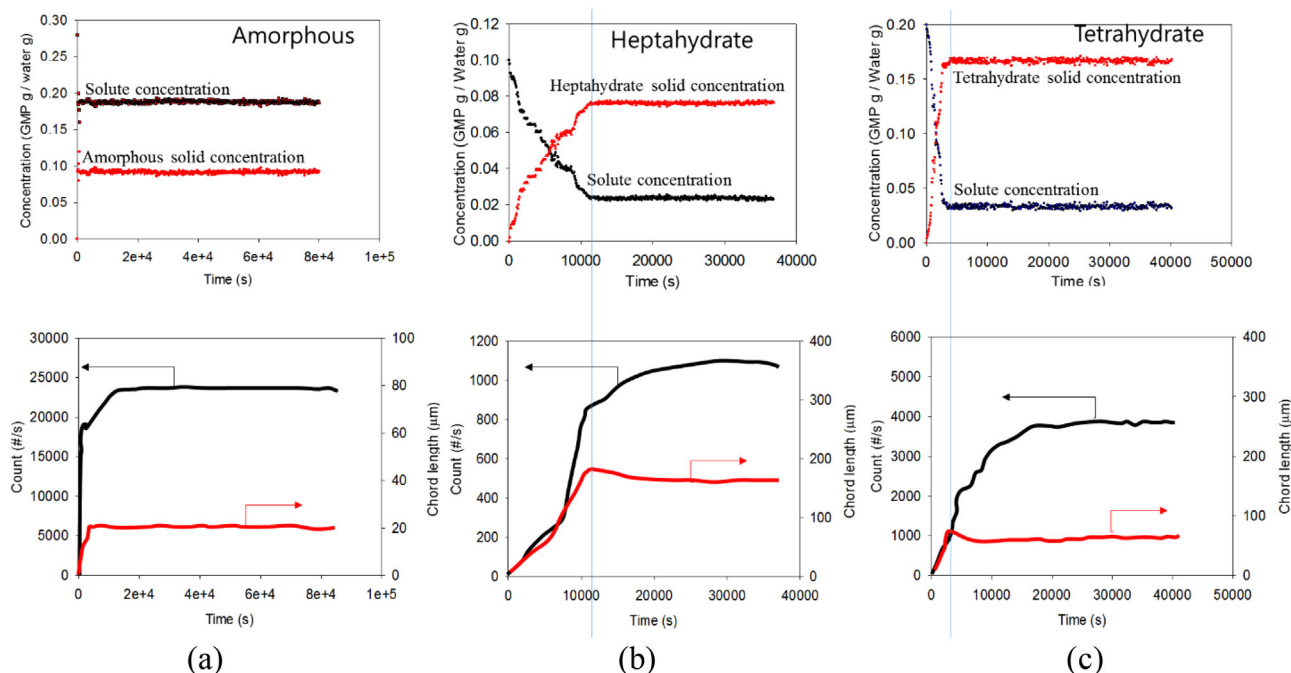


Figure 8. Preparation of amorphous, heptahydrate, and heptahydrate without transformation. Top graphs were calculated by calibration of Raman peaks. a–c) Top graphs show a) amorphous solid concentration, b) heptahydrate solid concentration, and c) tetrahydrate solid concentration with solute concentration, respectively; bottom graphs show counts of particle and chord length of a) amorphous solids, b) heptahydrate solids, and c) tetrahydrate solids over time, respectively. Blue bars indicate completion point for crystal growth of heptahydrate and tetrahydrate by variation of solute concentration and particle size with time.

growth rate is lower than the intrinsic dissolution rate. Most transformations expect this situation to be more common. Otherwise, the same considerations for the effect of surface area in the solid–liquid interface would be applied to this case. However, the initial total surface area of tetrahydrate is similar to that of heptahydrate and is estimated from the particle size distribution. Therefore, growth-controlled transformation can explain this case.

3.4.3. Heptahydrate–Tetrahydrate Transformation

As shown in Figure 7, after an induction period of 5650 s, tetrahydrate is formed and the concentration decreases to 0.060 g g^{-1} . The supersaturation consumption by dissolution of heptahydrate was about 0.0139 g g^{-1} , which was less than the total growth of tetrahydrate of 0.143 g g^{-1} .

There is a plateau region in the concentration of heptahydrate solid. As soon as the nucleation of the tetrahydrate started after the induction period, it behaved similarly to tetrahydrate–heptahydrate transformation. The solution concentration maintained the solubility of heptahydrate for 6800 s. In this transformation, the supersaturation consumed by crystal growth of tetrahydrate was 0.143 g g^{-1} per 1990 s, and the total dissolution of heptahydrate was 0.139 g g^{-1} per 1689 s. Therefore, the rate of supersaturation consumption by nucleation growth is smaller than that by dissolution. This case appears as a nucleation-growth-controlled transformation. From the viewpoint of the transformation mechanism, there is no change in particle size,

number of particles, or particle size distribution over the entire period, and the transformation from heptahydrate to tetrahydrate occurs. This phenomenon requires a driving force for nucleation of tetrahydrate, because the difference in solubility between the two hydrates is very small. One possibility of explaining it is a surface nucleation. The presence of a surface may be necessary to reduce the energy barrier for nucleation and to promote nucleation of the tetrahydrate. At this point, a higher concentration appears on the surface of the dissolved heptahydrate crystals compared to the solution, and, as a result, nucleation of tetrahydrate on the surface of the heptahydrate may be activated. A higher concentration of heptahydrate surface cannot induce nucleation of tetrahydrate on the same surface, because there is no driving force for heptahydrate dissolution prior to tetrahydrate nucleation. The transformation of the hydrate is energetically more likely to form nuclei at the interface. Similar results were reported in hydrate–anhydrate transformation.^[34–36]

3.5. Preparation of Amorphous, Heptahydrate, and Tetrahydrate without Transformation

Figure 8 shows solid phase concentration, solution concentration, particle size, and number of particles with elapsed time under various conditions. The equilibrium concentration of the amorphous solid was established immediately after the addition of antisolvent. The solution concentration was 0.088 g g^{-1} , and the amorphous solid concentration was 0.212 g g^{-1} . It remained amorphous without transformation for 28 h. The particle size

was 11 μm , and the number of counts was constant at 22 300 # s^{-1} (number count rate by FBRM).

Heptahydrate was crystallized immediately after the addition of the antisolvent at an initial concentration of 0.1 g g^{-1} . Over 11 000 s, the solution concentration decreased from 0.1 to 0.023 g g^{-1} , and the heptahydrate solid concentration increased to 0.077 g g^{-1} . Heptahydrate was maintained without transformation for 10 h. The particle size was 32 μm , and the number of particles was constant at 9500 # s^{-1} .

The tetrahydrate was crystallized immediately after the addition of the antisolvent at a temperature of 50 $^{\circ}\text{C}$ and an initial concentration of 0.2 g g^{-1} . Over a period of 3400 s, the solution concentration decreased from 0.2 to 0.032 g g^{-1} , and the tetrahydrate solid concentration increased to 0.168 g g^{-1} . The tetrahydrate was maintained without transformation for 10 h. The particle size was 72 μm , and the number of count was constant at 3900 # s^{-1} .

Therefore, in order to intentionally prepare either a metastable form or a stable form, the relationship between supersaturation and equilibrium concentration is necessary.

3.6. Effect of Antisolvent Adding Rate

The screening of GMP forms using antisolvent crystallization is affected by the antisolvent-to-solvent ratio, antisolvent feed rate, temperature, and initial concentration. Solution concentration-time profiles as a function of antisolvent feed rate at 20 and 50 $^{\circ}\text{C}$ are shown in Figure 9a,b, respectively. Nucleation, transformation, and growth were shown for the amorphous, heptahydrate, and tetrahydrate forms. Hydrates were formed at lower feed rates and lower concentrations. In some cases, the amorphous form was nucleated and then transformed to hydrate crystals. In the experiment at 20 $^{\circ}\text{C}$, hydrates were grown by nucleation of heptahydrates at the antisolvent feed rates of 0.9375 and 1.25 g min^{-1} with a feed concentration of 0.2 g g^{-1} , and at that of 38.0 g min^{-1} with a feed concentration of 0.1 g g^{-1} . Initially, amorphous solids were generated at 1.87–3.75 g min^{-1} , and transformed to heptahydrates after 2000 s. When the antisolvent feed rate is 38 g min^{-1} at 0.2 g g^{-1} , the amorphous form is first nucleated, and the solution concentration is maintained at the highest plateau for 4000 s, and then transformation into heptahydrate occurs. At 50 $^{\circ}\text{C}$, pure amorphous solid was prepared without transformation at an initial concentration of 0.3 g g^{-1} and an addition rate of 38.0 g min^{-1} . Pure tetrahydrate solids were obtained with transformation at the methanol fraction of 0.67. Heptahydrate-to-tetrahydrate and tetrahydrate-to-heptahydrate transformations were produced at methanol fractions of 0.33 and 0.5, respectively.

Figure 10a,b shows the plots of solution concentration against the methanol fraction for methanol feed rates at 20 and 50 $^{\circ}\text{C}$, respectively. As can be seen in Figure 10a, heptahydrate was nucleated at a methanol fraction of 0.183, and 0.208 for antisolvent addition rates of 0.9375 and 1.25 g min^{-1} , respectively, and then grown without transformation. Despite highest addition rate (38 g min^{-1}), at initial concentrations of 0.15 and 0.1 g g^{-1} , nucleation of heptahydrate occurred at methanol fractions of 0.161 and 0.155, respectively. An amorphous solid was formed at a methanol fraction of 0.32, at an addition rate of 3.75 g g^{-1} , and then transformed to heptahydrate at a methanol fraction of 0.50.

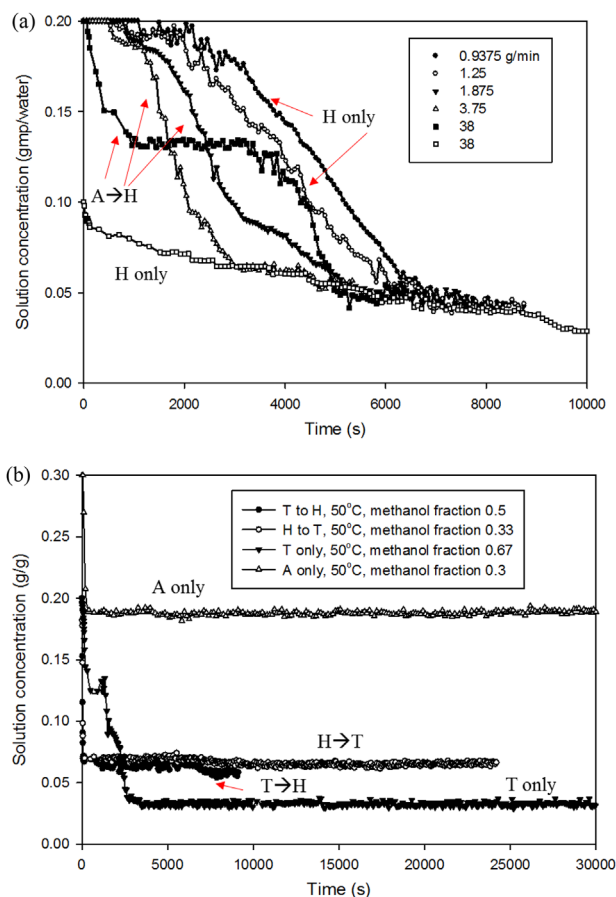


Figure 9. Variation of solution concentration with time for selective formation: a) 20 $^{\circ}\text{C}$ and b) 50 $^{\circ}\text{C}$. (A, H, and T stand for amorphous, heptahydrate, and tetrahydrate, respectively.)

After amorphous formation, the concentration decreased close to the solubility of heptahydrate by dissolution and growth. Heptahydrate was generated at an initial concentration of 0.1 g g^{-1} and a methanol fraction of 0.26 without transformation.

As can be seen in Figure 10b, which is the result for 50 $^{\circ}\text{C}$, the amorphous form was formed in a methanol fraction of 0.34, at an addition rate of 38 g min^{-1} , and an initial concentration of 0.3, and remained without transformation. The tetrahydrate was nucleated at a methanol fraction of 0.19 and at an addition rate of 3.8 g min^{-1} , and was grown without transformation. The transformation from the heptahydrate form to the tetrahydrate form occurred at a methanol fraction of 0.20, and the transformation from the tetrahydrate to the heptahydrate form occurred at a methanol fraction of 0.14. These results were similar to the hydrate formation behavior of taltirelin in batch crystallization.^[22] Finally from Figures 9 and 10, the supersaturation can be calculated by the difference between the metastable concentration C_{met} and the solubility C^* . It is applicable for the selective preparation of amorphous, heptahydrate, and tetrahydrate solids. Details on it will be reported in subsequent studies.

After nucleation, the concentration decreased to a more stable form of solubility due to the reduced supersaturation induced by crystal growth. The faster addition rate leads to the higher

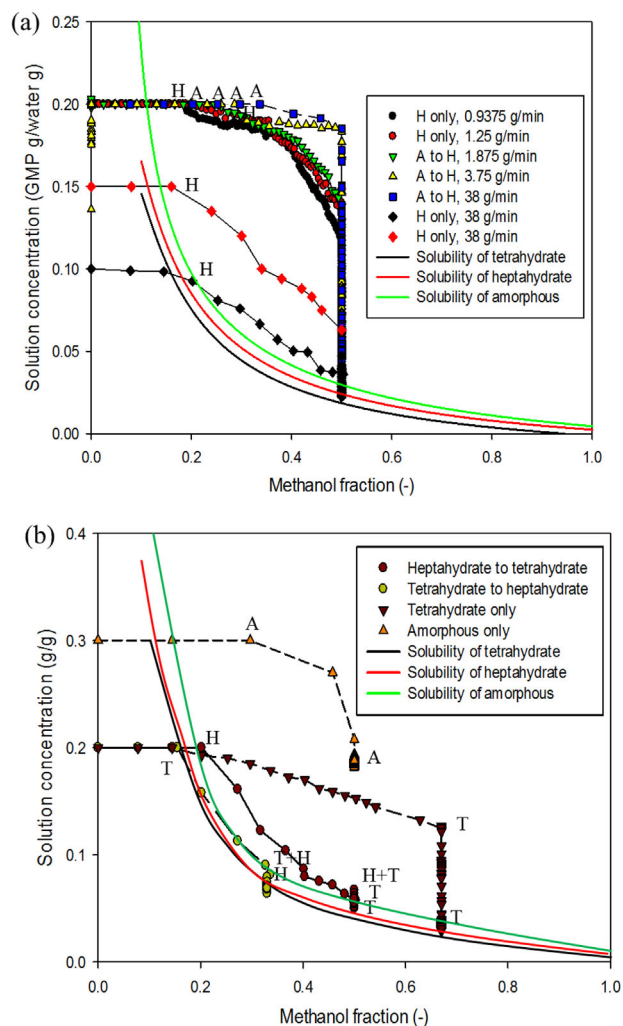


Figure 10. Solution concentration against methanol fraction for amorphous, heptahydrate, and tetrahydrate formations: a) 20 °C and b) 50 °C. (A, H, and T stand for amorphous, heptahydrate, and tetrahydrate, respectively.)

supersaturation. Thus, the amorphous form nucleated at a faster addition rate at the same solution concentration, whereas the hydrate crystals formed at a slower addition rate. The induction time was affected by supersaturation, which was related to the addition rate of antisolvent.

4. Conclusion

The formation of GMP solid forms was successfully monitored in-line by Raman spectroscopy and FBRM in an antisolvent crystallization process. The calibration and models built in this study can be used to measure the concentration of the solution and solid forms during crystallization and transformation. Faster addition of the antisolvent leads to a wider metastable zone as expected to favor the formation of the amorphous due to higher supersaturation. The effect of solvent/antisolvent ratio on solubility and supersaturation was studied. Phase transformation, maximum supersaturation, and selective preparation of GMP

solid forms were grasped. By adjusting the concentration, temperature, and solvent/antisolvent ratio, the preparation of the different solid forms with and without transformation was established. Therefore, a screening of amorphous, heptahydrate, and tetrahydrate of GMP was successfully established by knowing the metastable supersaturation of each of the forms.

The results demonstrate that amorphous–crystalline hydrate transformation consists of four stages, which are the nucleation of the amorphous form, pretransformation of the amorphous form, the nucleation of hydrate and dissolution of the amorphous form, and the growth of hydrate crystal. The rate-controlling step is the dissolution of the amorphous form. The transformation between heptahydrate and tetrahydrate forms is a nucleation-growth-controlled step. It was possible to control selectively the solid forms of GMP by referring to the supersaturation and the solubility data. This phenomenon requires a driving force for nucleation of tetrahydrate, because the difference in solubility between the two hydrates is very small. One possibility of explaining this is surface nucleation. The presence of a surface may be necessary to reduce the energy barrier for nucleation and to promote nucleation of the tetrahydrate. At this point, a higher concentration appears on the surface of the heptahydrate crystals that are dissolved compared to the solute concentration. As a result, nucleation of tetrahydrate on the surface of the heptahydrate can be activated.

Supporting Information

Supporting Information is available from the Wiley Online Library or from the author.

Acknowledgements

Open access funding enabled and organized by Projekt DEAL.

Conflict of Interest

The authors declare no conflict of interest.

Data Availability Statement

The data that support the findings of this study are available from the corresponding author upon reasonable request.

Keywords

amorphous, crystallization, hydrates, phase transformation

Received: August 26, 2021

Revised: December 1, 2021

Published online:

- [1] J. Ulrich, *Chem. Eng. Technol.* **2003**, *26*, 832.
- [2] B. Bechtloff, S. Nordhoff, J. Ulrich, *Cryst. Res. Technol.* **2001**, *36*, 1315.
- [3] N. J. Babu, A. Nangia, *Cryst. Growth Des.* **2011**, *11*, 2662.

- [4] B. Varsha, L. P. Pokharkar, M. N. P. Mandpe, A. A. Ambike, K. R. Mahadik, A. Paradkar, *Powder Technol.* **2006**, 167, 20.
- [5] P. Kanaujia, P. Poovizhi, W. K. Ng, R. B. H. Tan, *Powder Technol.* **2015**, 285, 2.
- [6] H. G. Brittain, *Polymorphism in Pharmaceutical Solids*, 2nd ed., Marcel Dekker, New York **2009**.
- [7] B. Shah, V. K. Kakumanu, A. K. Bansal, *J. Pharm. Sci.* **2006**, 95, 1641
- [8] T. Ishiguro, F. Hirayama, D. Iohara, H. Arima, K. Uekama, *Eur. J. Pharm. Sci.* **2010**, 39, 248.
- [9] T. N. P. Nguyen, K. J. Kim, *Int. J. Pharm.* **2008**, 364, 1.
- [10] J. J. Lu, J. Ulrich, *Cryst. Res. Technol.* **2005**, 40, 839.
- [11] K. J. Kim, M. F. Doherty, *AIChE J.* **2015**, 61, 1372.
- [12] J. M. Vaughn, J. T. McConville, M. T. Crisp, K. P. Johnston, R. O. Williams, III, *Drug Dev. Ind. Pharm.* **2006**, 32, 559.
- [13] R. Ledesma-Amaro, A. Jiménez, M. A. Santos, J. L. Revuelta, *Process Biochem.* **2013**, 48, 1263.
- [14] S. B. Zimmerman, *J. Mol. Biol.* **1976**, 106, 663.
- [15] S. Katti, T. Seshadri, M. Viswamitra, *Curr. Sci.* **1980**, 49, 533.
- [16] F. Zou, W. Zhuang, J. Wu, J. Zhou, P. Yang, Q. Liu, Y. Chen, H. Ying, *Ind. Eng. Chem. Res.* **2015**, 54, 137.
- [17] F. Zou, Q. Chen, P. Yang, J. Zhou, J. Wu, W. Zhuang, H. Ying, *Ind. Eng. Chem. Res.* **2017**, 56, 8274.
- [18] F. Zou, W. Zhuang, Q. Chen, P. Yang, C. Lin, P. Jiao, J. Zhou, J. Wu, H. Ying, *CrystEngComm* **2016**, 18, 6653.
- [19] R. Zhang, J. Ma, J. Li, Y. Jiang, M. Zheng, *Fluid Phase Equilib.* **2011**, 303, 35.
- [20] A. Salari, R. E. Young, *Int. J. Pharm.* **1998**, 163, 157.
- [21] M. Blanco, D. Valdés, I. Llorente, M. Bayod, *J. Pharm. Sci.* **2005**, 94, 1336.
- [22] D. L. T. Nguyen, K. J. Kim, *Chem. Eng. Technol.* **2015**, 38, 1059.
- [23] W. Su, H. Hao, B. Glennon, M. Barrett, *Cryst. Growth Des.* **2013**, 13, 5179.
- [24] S. C. Barthe, M. A. Grover, R. W. Rousseau, *Cryst. Growth Des.* **2008**, 8, 3316.
- [25] J. Ulrich, C. Strege, *J. Cryst. Growth* **2002**, 237, 2130.
- [26] W. Omar, S. Al-Sayed, A. Sultan, J. Ulrich, *Cryst. Res. Technol.* **2008**, 43, 22.
- [27] W. Omar, J. Ulrich, *Cryst. Growth Des.* **2006**, 6, 1927.
- [28] W. Omar, J. Ulrich, *Cryst. Res. Technol.* **2007**, 42, 432.
- [29] J. Kim, J. Ulrich, *Chem. Eng. Technol.* **2021**, <https://doi.org/10.1002/ceat.202100260>.
- [30] J. Heinrich, J. Ulrich, *Chem. Eng. Technol.* **2012**, 35, 967.
- [31] H. O. Yang, J. H. Kim, K. J. Kim, *Propellants, Explos., Pyrotech.* **2020**, 45, 422.
- [32] L. Wantha, A. E. Flood, *Chem. Eng. Technol.* **2013**, 36, 1313.
- [33] M. A. O'Mahony, A. Maher, D. M. Croker, Å. C. Rasmuson, B. K. Hodnett, *Cryst. Growth Des.* **2012**, 12, 1925.
- [34] D. Croker, B. K. Hodnett, *Cryst. Growth Des.* **2010**, 10, 2806.
- [35] M. A. O'Mahony, C. C. Seaton, D. M. Croker, S. Veessler, Å. C. Rasmuson, B. K. Hodnett, *Cryst. Growth Des.* **2013**, 13, 1861.
- [36] A. Maher, D. M. Croker, Å. C. Rasmuson, B. K. Hodnett, *Cryst. Growth Des.* **2012**, 12, 6151.